

# Hydrogen-Location-Sensitive Modulation of the Redox Reactivity for Oxygen-Deficient TiO<sub>2</sub>

Yao Guo<sup>†‡</sup>, Shunwei Chen<sup>†</sup>, Yaoguang Yu<sup>\*†</sup>, Haoran Tian<sup>†</sup>, Yanling Zhao<sup>†‡</sup>, Ji-Chang Ren<sup>†</sup>, Chao Huang<sup>†</sup>, Haidong Bian<sup>#</sup>, Miaoyan Huang<sup>†</sup>, Liang An<sup>‡</sup>, Yangyang Li<sup>#</sup>, Ruiqin Zhang<sup>\*†§</sup>

<sup>†</sup>Department of Physics, City University of Hong Kong, Hong Kong SAR, P. R. China

<sup>‡</sup>Shenzhen Research Institute, City University of Hong Kong, Shenzhen, P. R. China

<sup>‡</sup>Nano and Heterogeneous Materials Center, School of Materials Science and Engineering, Nanjing University of Science and Technology, Nanjing, Jiangsu, P. R. China

<sup>#</sup>Department of Materials Science and Engineering, City University of Hong Kong, Hong Kong SAR, P. R. China

<sup>‡</sup>Department of Mechanical Engineering, The Hong Kong Polytechnic University, Hong Kong SAR, P. R. China

<sup>§</sup>Beijing Computational Science Research Center, Beijing, P. R. China

## Supporting Information Placeholder

**ABSTRACT:** The hydrogenated black TiO<sub>2</sub> is receiving ever-increasing attention, primarily due to the ability of capturing low energy photons in the solar spectrum and the highly efficient redox reactivity for solar-driven water splitting. However, an in-depth understanding of the physical insight into the redox reactivity is still missing. In this work, we conducted the density functional theory study with Hubbard U correction (DFT+U) based on the model obtained from spectroscopic and aberration-corrected scanning transmission electron microscopy (AC-STEM) characterizations to reveal the synergy of H heteroatoms located at different surface sites where six-coordinated Ti (Ti<sub>6C</sub>) atom is converted from an inert trapping site to an interchange site of the photoexcited electrons. This in-depth understanding may be applicable to the rational design of highly efficient solar-harvesting catalysts.

TiO<sub>2</sub> has become one of the most extensively investigated photoactive materials for decades, especially in the application of energy and environmental fields.<sup>1–5</sup> There was a time that harvesting solar energy by using TiO<sub>2</sub> materials was restricted by their intrinsic wide band gaps (3.20 eV for anatase phase and 3.03 eV for rutile phase).<sup>6,7</sup> Fortunately, this barrier is overcome by creating disordered layer on the surface of TiO<sub>2</sub>, while the black hydrogenated TiO<sub>2</sub> is regarded as the landmark.<sup>8</sup> Subsequent researches reveal the hydrogen species play crucial roles not only in cutting off Ti-O bonds but also in tuning the bulk electronic structures to promote the charge separation.<sup>9</sup> However, the in-depth understanding of the physical insight into the redox reactivity, which implies the interaction (especially the charge transfer) between the active surface and the adsorbed reactants, is still lacking. The redox reactivity of photocatalysts is governed by the surface atomic arrangement along with the surface electronic structures at most scenes. The major challenge of investigating the redox reactivity of hydrogenated TiO<sub>2</sub> is the scarcity of convincing surface models.<sup>10,11</sup> One strategy is the utilization of well-investigated models to describe the disordered structure on the surface of black TiO<sub>2</sub>, such as amorphous titania. Unfortunately, it has been proved by Park and coworkers that the atomic arrangement of the disordered shell on the surface

of black TiO<sub>2</sub> is quite different from amorphous titania.<sup>12</sup>

As an alternative approach, if the disordered layer can be confined to several atomic layers on the surface of hydrogenated TiO<sub>2</sub>, a convincing model can be developed through elaborating spectroscopic and electron microscopic characterizations. Density functional theory (DFT) studies can be performed thereby revealing the redox reactivity of hydrogenated TiO<sub>2</sub> at a quantum level. Herein, an ultrathin disordered shell (2–4 atomic layers) on the surface of hydrogenated TiO<sub>2</sub> was prepared. The locations of H heteroatoms were monitored combining both spectroscopic and advanced aberration-corrected scanning transmission electron microscopy (AC-STEM) characterizations. The subsequent DFT studies with Hubbard U correction (DFT+U) unveil that the redox reactivity is sensitive to the locations of H heteroatoms on the surface of hydrogenated TiO<sub>2</sub>, which is further endorsed by the enhanced performance of solar-driven water splitting.

In a typical synthetic procedure, P25 powder was treated in a diluted hydrogen atmosphere for 15 min (denoted as H-15, other samples are abbreviated analogously) to obtain the confined disordered layer (Section I in SI). By means of the electron energy loss spectroscopy (EELS), the spatial distribution of Ti<sup>3+</sup> species within a particle region was obtained (Figure 1a). Compared with the data collected in the bulk region, there is an obvious shift of the Ti-L<sub>2,3</sub> edges towards the low energy loss direction for the surface component (Figure 1b). This shift indicates the oxygen vacancies associated with Ti<sup>3+</sup> species are predominantly distributed at the surface region.<sup>13,14</sup> As a reference, the synchronously collected O-K edges keep the same position among all the sampling points, demonstrating the intact valence state of O species (Figure 1c). Subsequently, a high-resolution HAADF-STEM image of H-15 sample was obtained to delineate the hydrogenated region (Figure 1d). The image with atomic resolution extracted from the cyan frame in Figure 1e further displays that the interplanar spacings of 0.239 and 0.234 nm with an included angle of 60.1° match well with the spatial geometry of {004} (*d* = 0.238 nm) and {112} (*d* = 0.233 nm) planes in anatase TiO<sub>2</sub>. Moreover, there is a perfectly one-to-one correspondence between the light spots in the HAADF-

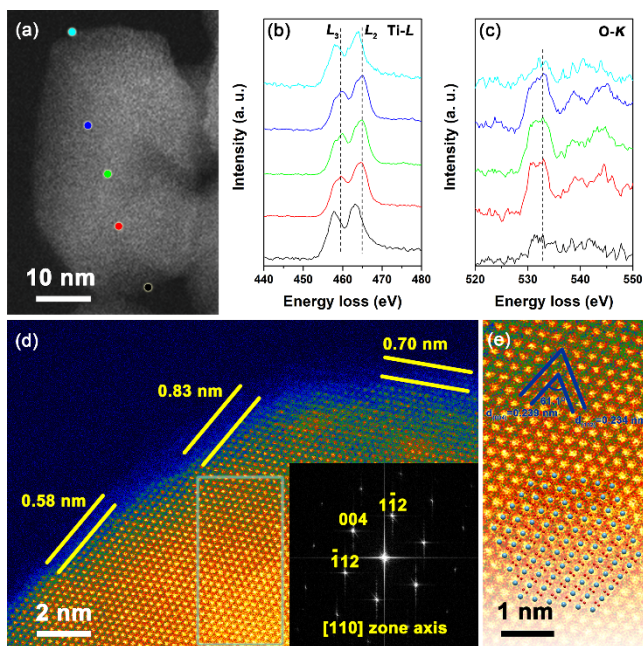


**Figure 1.** AC-STEM characterizations of the H-15 sample: a) HAADF-STEM image marked with the positions where EELS spectra were recorded. EELS spectra of b) Ti  $L_{2,3}$  and c) O-K edges. d) Atomic-resolution HAADF-STEM image embedded with corresponding FFT pattern. e) Image enlarged from the cyan frame marked in d).

STEM image and the Ti atoms in the inserted model, which reveals an unaffected bulk structure during the hydrogenation.<sup>15</sup> Based on the above observation, the disordered layer induced by hydrogenation is measured to be 0.58–0.83 nm, which corresponds to 2–4 atomic layers by taking the interplanar spacings of {004} and {112} planes into account.

In order to provide a solid evidence to the presence of  $Ti^{3+}$  species, X-ray photoelectron spectroscopy (XPS) was introduced (Figure 2a and Figure S1). The binding energies of Ti 2p core levels at 464.2 eV and 458.5 eV in all the samples can be assigned to the photoelectrons from Ti 2p<sub>1/2</sub> and Ti 2p<sub>3/2</sub> spin-orbital splittings of  $Ti^{4+}$  species.<sup>16,17</sup> In contrast, binding energies of 463.1 eV and 457.3 eV ascribed to  $Ti^{3+}$  species are only observed in hydrogenated samples.<sup>18</sup> This result indicates the  $Ti^{3+}$  species (induced by oxygen vacancies at most scenes) are generated during the hydrogenation process. As an accurate tool to detect the unpaired electron spins, electron paramagnetic resonance (EPR) was used to further probe  $Ti^{3+}$  species over hydrogenation time (Figure 2b). The g-tensor of 1.996 assigned to  $Ti^{3+}$  species can be observed in hydrogenated samples,<sup>19</sup> while the EPR signal in the P25 sample is absent. Besides, the EPR signal of the H-120 sample is stronger than the H-15 sample, which confirms the generation of  $Ti^{3+}$  species during hydrogenation. To locate H heteroatoms in the hydrogenated layer,  $^1H$  nuclear magnetic resonance ( $^1H$  NMR) was conducted (Figure 2c). For the pristine P25 sample, two peaks of chemical shift ( $\delta$ ) at 5.2 and 1.8 ppm are assigned to the H heteroatoms in the surface-adsorbed water molecule and H-O<sub>3C</sub> group on the surface of pristine  $TiO_2$ , respectively.<sup>20,21</sup> After hydrogenation for 15 min, the former two peaks of  $\delta$  are replaced for three new peaks. The peaks of  $\delta$  at 0.4 and 6.3 ppm can be assigned to H heteroatoms in H-O<sub>3C</sub> and H-O<sub>2C</sub> groups on the hydrogenated surface, respectively.<sup>22</sup> Noting that an overlapped shoulder peak of  $\delta$  at ca. -0.6 ppm is observed, which has not been reported yet. It is widely accepted the presence of Ti-H-Ti bonds in

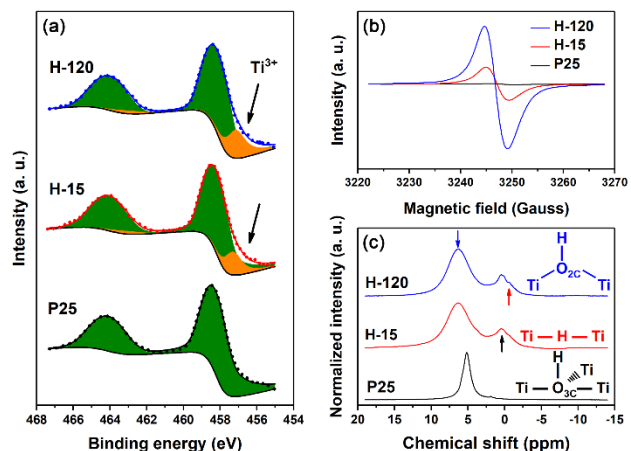


**Figure 2.** a) XPS spectra of Ti 2p core levels, b) EPR spectra, and c)  $^1H$  NMR spectra of pristine P25, H-15, and H-120 samples. The H-O<sub>3C</sub> group is a H heteroatom connected with a three coordinated O atom; the H-O<sub>2C</sub> group is a H heteroatom connected with a two coordinated O atom; and the H<sub>0</sub> heteroatom is a H heteroatom located in the oxygen vacancy in the form of Ti-H-Ti bond.

hydrogenated  $TiO_2$ .<sup>9</sup> Generally, the  $\delta$  value of  $^1H$  NMR for transition-metal hydrides is negative, because the electronegativity of H is more negative than most of the transition-metals.<sup>23</sup> As for our case, the more negative electronegativity of H (2.1) compared with Ti (1.5) achieves the  $\delta$  value of -0.6 ppm for H<sub>0</sub> heteroatom.<sup>24</sup> When prolonging the hydrogenation time to 120 min, the peak of  $\delta$  at -0.6 ppm is more obvious (Figure S2). Consequently, there are three types of H heteroatoms on the surface of hydrogenated  $TiO_2$ , and the amount of H<sub>0</sub> heteroatom increases with prolonging hydrogenation time.

Howbeit the detailed surface atomic arrangement of the hydrogenated  $TiO_2$  is obtained, the foremost task is to evaluate the stability of the H<sub>0</sub>, H-O<sub>2C</sub>, and H-O<sub>3C</sub> groups because the steady-state redox reactivity depends on a robust bonding. The order of the relative stability for H heteroatoms located at different sites is calculated in the sequence of H<sub>0</sub>, H-O<sub>2C</sub>, and H-O<sub>3C</sub> (Figure 3a). Considering the similar contribution of H heteroatoms in H-O<sub>2C</sub> and H-O<sub>3C</sub> groups to the conduction band associated with the low stability of the H heteroatom in the H-O<sub>3C</sub> group, the effect of the H heteroatom location on the redox reactivity is analyzed based on H heteroatoms in H<sub>0</sub> and H-O<sub>2C</sub> groups (Figure S3-S5). By comparing the PDOS of intact (101) surface model and H<sub>0</sub>+H-O<sub>2C</sub> model of oxygen-deficient (101) surface (Figure 3b), it is found that, firstly, the absorption edges of hydrogenated  $TiO_2$  come out of the electron excitation from the valence band to the states above the Fermi level (path I in Figure 3c); and secondly, the enhanced absorbance beyond the absorption edges is ascribed to the excitation of electrons from the states in the conduction band below the Fermi level to the states above (path II in Figure 3c).<sup>25</sup> Unfortunately, through evaluating the H heteroatom induced surface structural deformation, the single H<sub>0</sub> heteroatom modified surface is found to be inhibited to the surface charge separation (Section II in SI).<sup>6,26,27</sup> Furthermore, the unoccupied 1s orbital of H heteroatom in the H-O<sub>2C</sub> group is mainly distributed in the deep

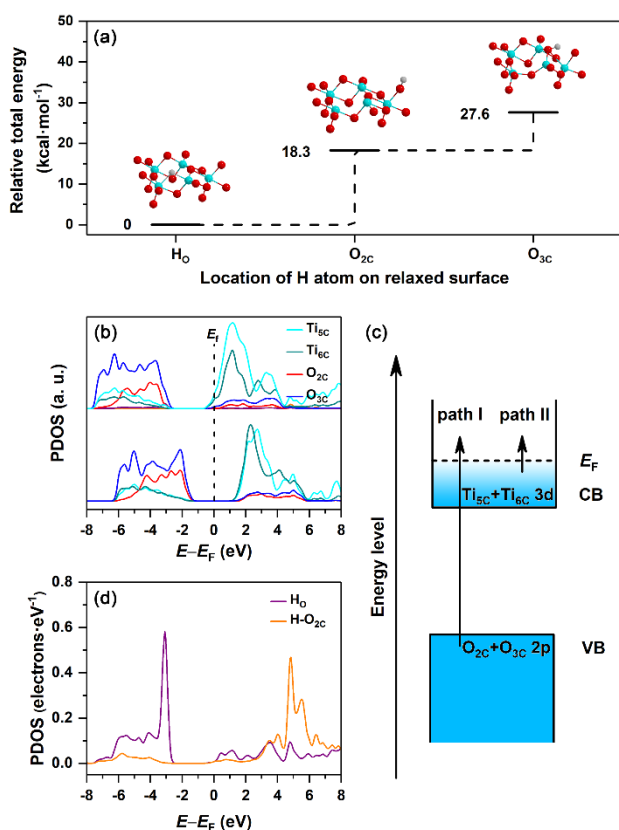


**Figure 3.** a) Relationship between the relative total energy and the location of the H heteroatom on the oxygen-deficient (101) surface of anatase TiO<sub>2</sub>. b) Surface PDOS of intact (101) surface of anatase TiO<sub>2</sub> (lower) and oxygen-deficient (101) surface of anatase TiO<sub>2</sub> with H<sub>0</sub> and H-O<sub>2C</sub> groups (H<sub>0</sub>+H-O<sub>2C</sub> model, upper). c) Schematic energy level diagram of the hydrogenated oxygen-deficient TiO<sub>2</sub>. d) Surface PDOS of the H heteroatoms in the H<sub>0</sub>+H-O<sub>2C</sub> model.

level of the conduction band, which seems tangential to the surface electronic structures (Figure 3d). Namely, a potential synergy between H heteroatoms in H<sub>0</sub> and H-O<sub>2C</sub> groups may finally contribute to the redox reactivity.

To attest the results of the DFT+U calculation, the behavior of the photoexcited electron is monitored by the UV-vis spectrum (Figure 4a). The optical band gaps of H-15 and H-120 samples (2.82 and 2.78 eV) match well with the theoretical result (2.79 eV) extracted from the PDOS of the H<sub>0</sub>+H-O<sub>2C</sub> model (Figure S6), which endorses the validity of the model and the DFT+U method. Moreover, compared with the H-15 sample, the stronger absorption of the H-120 sample beyond the absorption edge demonstrates an obviously enhanced excitation of electrons from the states in the conduction band below the Fermi level to the states above (path II in Figure 3c). Noting that the penetration of Fermi level through the conduction band provides a shortcut for the recombination of photoexcited electrons with holes in the conduction band below the Fermi level. However, the steady-state photocurrent of the H-120 sample after 1000 s is 228 μA·cm<sup>-2</sup> comparing with 149 μA·cm<sup>-2</sup> for the H-15 sample (53% enhancement). Similar enhancement (62%) is also observed during the photocatalytic water splitting process (Figure S7 and S8). Accordingly, the redox reactivity of the hydrogenated surface based on a highly efficient charge transfer should play a dominant role in the solar-driven water splitting reaction.

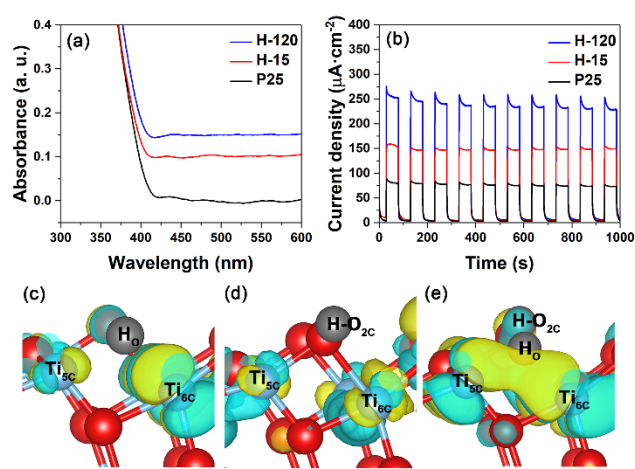


**Figure 4.** a) UV-vis spectra and b) *I-t* curves of P25, H-15, and H-120 samples used for chopped illumination. Orbital spatial-distribution of the CBM by DFT+U calculations for c) H<sub>0</sub> model, d) H-O<sub>2C</sub> model, and e) H<sub>0</sub>+H-O<sub>2C</sub> model.

It is widely accepted that Ti<sub>5C</sub> atoms on the (101) surface of anatase TiO<sub>2</sub> function as the adsorption site and electron transfer channel for water splitting reaction, namely the reactivity of anatase TiO<sub>2</sub> depends on the number of Ti<sub>5C</sub> atoms.<sup>28,29</sup> In contrast, Ti<sub>6C</sub> atoms are inert due to both the steric hindrance and saturated coordination. Based on the surface PDOS diagram (Figure 3b and Figure S5), the CBM of all the H<sub>0</sub>, H-O<sub>2C</sub>, and H<sub>0</sub>+H-O<sub>2C</sub> models involve Ti<sub>5C</sub> and Ti<sub>6C</sub> atoms. Notwithstanding the overlapped energy levels of orbitals (in CBM) ascribed to Ti<sub>5C</sub> and Ti<sub>6C</sub> atoms, these orbitals are mainly localized at the Ti<sub>6C</sub> site with a small fraction localized at the Ti<sub>5C</sub> site in the single H heteroatom modified oxygen-deficient (101) surface of anatase TiO<sub>2</sub> (Figure 4c, d). Considering the inert Ti<sub>6C</sub> atom during the PEC reaction, the limited orbital distribution of CBM at the Ti<sub>5C</sub> site will result in a mediocre redox reactivity. Exceptionally, the orbital distribution of the CBM in the H<sub>0</sub>+H-O<sub>2C</sub> model is extensively delocalized between Ti<sub>5C</sub> and Ti<sub>6C</sub> atoms (Figure 4e), exhibiting a synergy between H heteroatoms in H<sub>0</sub> and H-O<sub>2C</sub> groups. Moreover, by ruling out the potential influence of carrier lifetime (Section III in SI), it is confirmed that this synergy contributes to a considerable extra supply of photoexcited electrons from Ti<sub>6C</sub> to Ti<sub>5C</sub> atoms, thus achieving a remarkable improvement in the redox reactivity.

In conclusion, the origin of the outstanding redox reactivity of the hydrogenated TiO<sub>2</sub> for solar-driven water splitting has been disclosed to be the synergy between H heteroatoms in H<sub>0</sub> and H-O<sub>2C</sub> groups. The synergy results in an extensively delocalized orbital distribution of the CBM between surface Ti<sub>5C</sub> and Ti<sub>6C</sub> atoms. This delocalization converts the Ti<sub>6C</sub> atom from an inert site to an interchange channel of photoexcited electrons to the active Ti<sub>5C</sub> atom, which remarkably improves the redox reactivity for solar-driven water splitting.

## ASSOCIATED CONTENT

### Supporting Information

The Supporting Information is available free of charge on the ACS Publications website.

Materials characterization; Photoelectrochemical measurements; Models and computational details; XPS survey spectra; <sup>1</sup>H NMR spectra; Surface PDOS; Tauc plots; Photocatalytic water splitting performance; Synthetic procedure and texture characterization;

## AUTHOR INFORMATION

### Corresponding Author

\*yaoguayu@cityu.edu.hk

\*aprqz@cityu.edu.hk

### ORCID

Yaoguang Yu: 0000-0002-8332-3985

Ruiqin Zhang: 0000-0001-6897-4010

### Notes

The authors declare no competing financial interests.

## ACKNOWLEDGMENT

This work was financially supported by the NSF of China (21601042), Science Technology and Innovation Committee of Shenzhen Municipality (JCYJ20170818104105891), and the “Hong Kong Scholars Program”. The authors thank Dr. S. V. Kershaw for the helpful discussion in time-resolved PL spectrum, Dr. F. Huang for the help in the preparation of the photoelectrodes, and Dr. F. X. Ma for the operation of the hydrogenation furnace.

## REFERENCES

- (1) Fujishima, A.; Honda, K. Electrochemical Photolysis of Water at a Semiconductor Electrode. *Nature* **1972**, *238*, 37–38.
- (2) Sambur, J. B.; Chen, T. Y.; Choudhary, E.; Chen, G. Q.; Nissen, E. J.; Thomas, E. M.; Zou, N. M.; Chen, P. Sub-Particle Reaction and Photocurrent Mapping to Optimize Catalyst-Modified Photoanodes. *Nature* **2016**, *530* (7588), 77–80.
- (3) Butburee, T.; Bai, Y.; Wang, H. J.; Chen, H. J.; Wang, Z. L.; Liu, G.; Zou, J.; Khemthong, P.; Lu, G. Q. M.; Wang, L. Z. 2D Porous TiO<sub>2</sub> Single-Crystalline Nanostructure Demonstrating High Photo-Electrochemical Water Splitting Performance. *Adv. Mater.* **2018**, *30* (21), 1705666.
- (4) Shalom, M.; Dor, S.; Rühle, S.; Grinis, L.; Zaban, A. Core/CdS Quantum Dot/Shell Mesoporous Solar Cells with Improved Stability and Efficiency Using an Amorphous TiO<sub>2</sub> Coating. *J. Phys. Chem. C* **2009**, *113* (9), 3895–3898.
- (5) Wang, Y. Q.; Gu, L.; Guo, Y. G.; Li, H.; He, X. Q.; Tsukimoto, S.; Ikuhara, Y.; Wan, L. J. Rutile-TiO<sub>2</sub> Nanocoating for a High-Rate Li<sub>4</sub>Ti<sub>5</sub>O<sub>12</sub> Anode of a Lithium-Ion Battery. *J. Am. Chem. Soc.* **2012**, *134* (18), 7874–7879.
- (6) Scanlon, D. O.; Dunnill, C. W.; Buckeridge, J.; Shevlin, S. A.; Logsdail, A. J.; Woodley, S. M.; Catlow, C. R. A.; Powell, M. J.; Palgrave, R. G.; Parkin, I. P.; Watson, G. W.; Keal, T. W.; Sherwood, P.; Walsh, A.; Sokol, A. A. Band Alignment between Anatase and Rutile TiO<sub>2</sub>. *Nat. Mater.* **2013**, *12*, 798–801.
- (7) Zhou, L. J.; Zhang, J.; Zhuo, Z. W.; Kou, L. Z.; Ma, W.; Shao, B.; Du, A. J.; Meng, S.; Frauenheim, T. Novel Excitonic Solar Cells in Phosphorene-TiO<sub>2</sub> Heterostructures with Extraordinary Charge Separation Efficiency. *J. Phys. Chem. Lett.* **2016**, *7* (10), 1880–1887.
- (8) Chen, X. B.; Liu, L.; Yu, P. Y.; Mao, S. S. Increasing Solar Absorption for Photocatalysis with Black Hydrogenated Titanium Dioxide Nanocrystals. *Science* **2011**, *331* (6018), 746–750.
- (9) Liu, L.; Yu, P. Y.; Chen, X. B.; Mao, S. S.; Shen, D. Z. Hydrogenation and Disorder in Engineered Black TiO<sub>2</sub>. *Phys. Rev. Lett.* **2013**, *111* (6), 065505.
- (10) Zhang, K.; Park, J. H. Surface Localization of Defects in Black TiO<sub>2</sub>: Enhancing Photoactivity or Reactivity. *J. Phys. Chem. Lett.* **2017**, *8* (1), 199–207.
- (11) Liu, X. Y.; Zhu, G. L.; Wang, X.; Yuan, X. T.; Lin, T. Q.; Huang, F.

- Q. Progress in Black Titania: A New Material for Advanced Photocatalysis. *Adv. Energy Mater.* **2016**, *6* (17), 1600452.
- (12) Zhang, K.; Wang, L. Y.; Kim, J. K.; Ma, M.; Veerappan, G.; Lee, C. L.; Kong, K. J.; Lee, H. Y.; Park, J. H. An Order/Disorder/Water Junction System for Highly Efficient Co-Catalyst-Free Photocatalytic Hydrogen Generation. *Energy Environ. Sci.* **2016**, *9* (2), 499–503.
  - (13) Gordon, T. R.; Cargnello, M.; Paik, T. J.; Mangolini, F.; Weber, R. T.; Fornasiero, P.; Murray, C. B. Nonaqueous Synthesis of TiO<sub>2</sub> Nanocrystals Using TiF<sub>4</sub> to Engineer Morphology, Oxygen Vacancy Concentration, and Photocatalytic Activity. *J. Am. Chem. Soc.* **2012**, *134* (15), 6751–6761.
  - (14) Lü, X. J.; Chen, A. P.; Luo, Y. K.; Lu, P.; Dai, Y. M.; Enriquez, E.; Dowden, P.; Xu, H. W.; Kotula, P. G.; Azad, A. K.; Yarotski, D. A.; Prasankumar, R. P.; Taylor, A. J.; Thompson, J. D.; Jia, Q. X. Conducting Interface in Oxide Homo Junction: Understanding of Superior Properties in Black TiO<sub>2</sub>. *Nano Lett.* **2016**, *16* (9), 5751–5755.
  - (15) Kawasaki, M.; Yamazaki, T.; Sato, S.; Watanabe, K.; Shiojiri, M. Atomic-Scale Quantitative Elemental Analysis of Boundary Layers in a SrTiO<sub>3</sub> Ceramic Condenser by High-Angle Annular Dark-Field Electron Microscopy. *Philos. Mag. A* **2001**, *81* (1), 245–260.
  - (16) Wang, Y.; Marquard, S. L.; Wang, D. G.; Dares, C.; Meyer, T. J. Single-Site, Heterogeneous Electrocatalytic Reduction of CO<sub>2</sub> in Water as the Solvent. *ACS Energy Lett.* **2017**, *2* (6), 1395–1399.
  - (17) Jiang, H. B.; Cuan, Q.; Wen, C. Z.; Xing, J.; Wu, D.; Gong, X. Q.; Li, C. Z.; Yang, H. G. Anatase TiO<sub>2</sub> Crystals with Exposed High-Index Facets. *Angew. Chem. Int. Ed.* **2011**, *50* (16), 3764–3768.
  - (18) Marshall, M. S. J.; Becerra-Toledo, A. E.; Marks, L. D.; Castell, M. R. Surface and Defect Structure of Oxide Nanowires on SrTiO<sub>3</sub>. *Phys. Rev. Lett.* **2011**, *107* (8), 086102.
  - (19) Zhou, X. M.; Zolnhofer, E. M.; Nguyen, N. T.; Liu, N.; Meyer, K.; Schmuki, P. Stable Co-Catalyst-Free Photocatalytic H<sub>2</sub> Evolution from Oxidized Titanium Nitride Nanopowders. *Angew. Chem. Int. Ed.* **2015**, *54* (45), 13385–13389.
  - (20) Jiang, Y. J.; Amal, R. Selective Synthesis of TiO<sub>2</sub>-Based Nanoparticles with Highly Active Surface Sites for Gas-Phase Photocatalytic Oxidation. *Appl. Catal. B Environ.* **2013**, *138–139*, 260–267.
  - (21) Liu, F.; Feng, N. D.; Wang, Q.; Xu, J.; Qi, G. D.; Wang, C.; Deng, F. Transfer Channel of Photoinduced Holes on a TiO<sub>2</sub> Surface As Revealed by Solid-State Nuclear Magnetic Resonance and Electron Spin Resonance Spectroscopy. *J. Am. Chem. Soc.* **2017**, *139* (29), 10020–10028.
  - (22) Crocker, M.; Herold, R. H. M.; Wilson, A. E.; Mackay, M.; Emeis, C. A.; Hoogendoorn, A. M. <sup>1</sup>H NMR Spectroscopy of Titania: Chemical Shift Assignments for Hydroxy Groups in Crystalline and Amorphous Forms of TiO<sub>2</sub>. *J. Chem. Soc. Faraday Trans.* **1996**, *92* (15), 2791–2798.
  - (23) Ruiz-Morales, Y.; Schreckenbach, G.; Ziegler, T. Origin of the Hydridic <sup>1</sup>H NMR Chemical Shift in Low-Valent Transition-Metal Hydrides. *Organometallics* **1996**, *15* (19), 3920–3923.
  - (24) Bergmann, D.; Hinze, J. Electronegativity and Molecular Properties. *Angew. Chem. Int. Ed.* **1996**, *35* (2), 150–163.
  - (25) Yu, Y. G.; Yang, X.; Zhao, Y. L.; Zhang, X. B.; An, L.; Huang, M. Y.; Chen, G.; Zhang, R. Q. Engineering the Band Gap States of the Rutile TiO<sub>2</sub>(110) Surface by Modulating the Active Heteroatom. *Angew. Chem. Int. Ed.* **2018**, *57* (28), 8550–8554.
  - (26) Setvin, M.; Franchini, C.; Hao, X. F.; Schmid, M.; Janotti, A.; Kaltak, M.; Van De Walle, C. G.; Kresse, G.; Diebold, U. Direct View at Excess Electrons in TiO<sub>2</sub> Rutile and Anatase. *Phys. Rev. Lett.* **2014**, *113* (8), 086402.
  - (27) Yu, Y. G.; Chen, G.; Wang, Q.; Li, Y. X. Hierarchical Architectures of Porous ZnS-Based Microspheres by Assembly of Heterostructure Nanoflakes: Lateral Oriented Attachment Mechanism and Enhanced Photocatalytic Activity. *Energy Environ. Sci.* **2011**, *4* (9), 3652–3660.
  - (28) Pan, J.; Liu, G.; Lu, G. Q.; Cheng, H. M. On the True Photoreactivity Order of {001}, {010}, and {101} Facets of Anatase TiO<sub>2</sub> Crystals. *Angew. Chem. Int. Ed.* **2011**, *50* (9), 2133–2137.
  - (29) Li, Y. F.; Liu, Z. P.; Liu, L. L.; Gao, W. G. Mechanism and Active Site of Photocatalytic Water Splitting on Titania in Aqueous Surroundings. *J. Am. Chem. Soc.* **2010**, *132* (37), 13008–13015.

